AGU PUBLICATIONS

Journal of Advances in Modeling Earth Systems

RESEARCH ARTICLE

10.1002/2017MS001104

Stratocumulus to Cumulus Transition by Drizzle

Takanobu Yamaguchi[1,2], **Graham Feingold**[2], **and Jan Kazil**[1,2]

[1]Cooperative Institute for Research in Environmental Sciences, University of Colorado, Boulder, Boulder, CO, USA, [2]NOAA Earth System Research Laboratory, Boulder, CO, USA

Key Points:
- Drizzle generated in penetrative cumulus below stratocumulus causes rapid transition to cumulus state
- The rapid transition is a result of precipitation scavenging of aerosol
- The rapid transition does not occur when cloud droplet number is specified

Correspondence to:
T. Yamaguchi,
tak.yamaguchi@noaa.gov

Citation:
Yamaguchi, T., Feingold, G., & Kazil, J. (2017). Stratocumulus to cumulus transition by drizzle. *Journal of Advances in Modeling Earth Systems*, *9*, 2333–2349. https://doi.org/10.1002/2017MS001104

Received 27 JUN 2017
Accepted 18 SEP 2017
Accepted article online 21 SEP 2017
Published online 24 OCT 2017

Abstract The stratocumulus to cumulus transition (SCT) is typically considered to be a slow, multiday process, caused primarily by dry air entrainment associated with overshooting cumulus, with minor influence of drizzle. This study revisits the role of drizzle in the SCT with large eddy simulations coupled with a two-moment bulk microphysics scheme that includes a budget on aerosol (N_a) and cloud droplet number concentrations (N_c). We show a strong precipitation-induced modulation of the SCT by drizzle initiated in penetrative cumulus under stratocumulus. Lagrangian SCT simulations are initiated with various, moderate N_a (100–250 cm^{-3}), which produce little to no drizzle from the stratocumulus. As expected, drizzle formation in cumuli is regulated by cloud depth and N_c, with stronger dependence on cloud depth, so that, for the current case, drizzle is generated in all simulations once cumulus clouds become sufficiently deep. The drizzle generated in the cumuli washes out stratocumulus cloud water and much of the aerosol, and a cumulus state appears for approximately 10 h. With additional simulations with a fixed N_c (100 cm^{-3}), we show that prediction of N_c is necessary for this fast SCT since it is a result of a positive feedback of collision-coalescence-induced aerosol depletion that enhances drizzle formation. A fixed N_c does not permit this feedback, and thus results in weak influence of drizzle on the SCT. Simulations with fixed droplet concentrations that bracket the time varying aerosol/drop concentrations are therefore not representative of the role of drizzle in the SCT.

1. Introduction

In the subtropics, where the Hadley circulation descends, marine stratocumulus clouds prevail over colder waters near the western flanks of the continents, while shallow cumulus clouds dominate further west, over warmer waters, following the equatorward branch of the Hadley circulation, also known as the trade winds. This transition between cloud types/regimes in the marine planetary boundary layer (PBL) is accompanied by large changes in cloud amount, thus generating significant interest in the underlying mechanism of the transition.

Focused efforts to elucidate the stratocumulus to cumulus transition (SCT) have been conducted via both observations (Albrecht et al., 1995; Bretherton & Pincus, 1995; de Roode & Duynkerke, 1997; Paluch & Lenschow, 1991; Pincus et al., 1997) and modeling (Bretherton, 1992; Bretherton et al., 1999; Bretherton & Wyant, 1997; Chung et al., 2012; de Roode et al., 2016; Krueger et al., 1995; McGibbon & Bretherton, 2017; Sandu et al., 2010; Sandu & Stevens, 2011; Stevens, 2000; van der Dussen et al., 2013; Wang et al., 1993; Wyant et al., 1997). According to the now largely accepted theory proposed by Bretherton (1992), Bretherton and Wyant (1997), and Wyant et al. (1997, hereafter W97), the SCT occurs due to advection of the cloud system over a continuously increasing sea surface temperature (SST), which promotes decoupling in the stratocumulus layer, the subsequent appearance of cumulus under stratocumulus, and then gradual dissipation of stratocumulus due to overshooting cumulus entrainment of dry free tropospheric air. The increasing latent heat flux associated with the warming SST plays a crucial role in generating decoupling that shifts convection from a radiative cooling driven, well-mixed stratocumulus regime to a surface driven, cumulus-favoring regime (W97). In the decoupled boundary layer, a weak stable layer appears below the stratocumulus cloud base, through which only cumulus can penetrate.

SCT theory has been suggested to apply to the four subtropical oceans; multiple reanalysis-derived SCT trajectories, Sandu et al. (2010) show that SCTs in these ocean basins share fundamental characteristics. By compositing trajectories in the northeast Pacific, Sandu and Stevens (2011, hereafter SS11) designed a 3

day Lagrangian large eddy simulation SCT case and demonstrated that the SCT is driven primarily by the SST gradient and that the time scale of the SCT is proportional to the initial lower tropospheric stability (i.e., in the stratocumulus regime). A recent large eddy simulation SCT intercomparison study (de Roode et al., 2016) comprising six models simulating SS11 shows consistency among the models, supporting SCT theory and SS11. One of the models that participated in that study is the model used here.

These studies have argued that precipitation associated with both drizzle in stratocumulus and in cumulus is not required for the SCT, and only creates minor modulation to the evolution of the SCT, with its primary influence on fractional cloudiness. In the past, drizzle was considered to play an important role in the SCT. Paluch and Lenschow (1991, henceforth PL91) suggested that the role of drizzle occurs in two ways: (i) drizzle tends to warm and dry the cloud layer, promoting stabilization across cloud base and (ii) drizzle promotes a conditionally unstable subcloud layer with respect to the surface layer. These result in a potential temperature profile characterized by an unstable layer capped by a stable layer. This condition favors moisture buildup near the surface until moist adiabatic conditions allow cumulus clouds to rise from the unstable layer and penetrate into the stable cloud layer, which eventually achieves a breakup of the upper stratocumulus layer. This mechanism would not occur in the absence of heavy drizzle, as corroborated by past studies.

Recently, Yamaguchi et al. (2015) reported that their control simulation, which is based on SS11, manifests a strong modulation of the SCT by precipitation near the end of the 3 day simulation, so that the time scale of the SCT is controlled by precipitation in addition to the initial lower tropospheric stability. Motivated by the discrepancy with SCT theory and a possible link to PL91's scenario, we carry out numerical simulations to study the role of precipitation in the SCT, how the emerging understanding differs from the standard theory, and why SS11 and the SCT intercomparison study of de Roode et al. (2016) did not observe a strong modulation of SCT by precipitation.

A description of our model and simulation cases is presented in the next section. Results with prognostic aerosol and cloud droplet number concentrations are shown in section 3. In section 4, results for additional simulations with a fixed cloud droplet number concentration are presented to study the impact of different microphysical treatments on the modulation of the SCT. A summary is given in section 5.

2. Large Eddy Simulations

Simulations are based on the 3 day Lagrangian SCT case developed by SS11. Initial profiles and the time evolution of the SST follow SS11, and subsidence follows Bretherton and Blossey (2014, hereafter BB14). The latter study modified subsidence from SS11 in order to achieve a better fit to the subsidence rate at the inversion height.

The System for Atmospheric Modeling (SAM) (Khairoutdinov & Randall, 2003), built with a finite difference representation of the anelastic system on the Arakawa C-grid spatial discretization, is employed. The third-order Adams-Bashforth time integration method (Durran, 1991) coupled with the second-order centered advection scheme is used for momentum, whereas the Euler time integration method with fifth-order monotonic advection scheme of Yamaguchi et al. (2011) is used for scalars. Diffusion is explicitly computed with the eddy coefficients obtained from the 1.5-order subgrid scale turbulence kinetic energy (TKE) scheme based on Deardorff (1980). The elliptic equation for the pressure perturbation is solved through fast Fourier transform.

A bin-emulating bulk two-moment microphysics scheme (Feingold et al., 1998; Wang & Feingold, 2009) represents cloud and rain water modes using lognormal functions with fixed geometric standard deviation of 1.2. The threshold between the two modes is a drop radius of 25 μm. Since large drizzle drops reside in the rain mode, we use rain and drizzle interchangeably in this study, without necessarily conforming to the meteorological distinction between drizzle and rain. In the scheme, a prognostic equation is solved for aerosol number concentration, N_a; a lognormal aerosol size distribution (ammonium sulfate) with geometric-mean diameter of 0.2 μm and geometric standard deviation of 1.5 is assumed. Supersaturation is calculated based on the balance of dynamical and microphysical source and sink terms over the course of a time step. Under supersaturated conditions aerosol particles are activated and removed from the aerosol population so that the reduction in N_a exactly balances the increase in cloud drop concentration, N_c. Similarly, drop

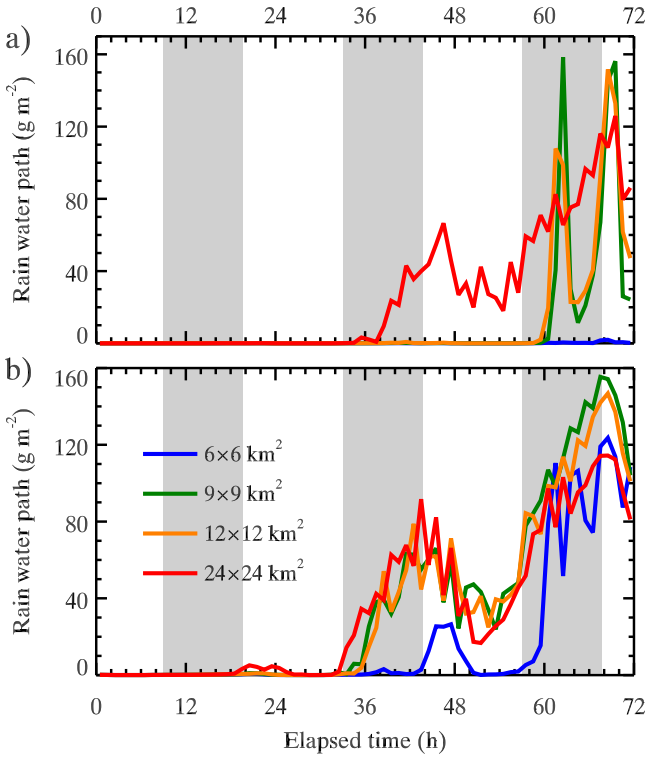

Figure 1. Time series of hourly averaged domain mean L_r for four horizontal domain sizes for (a) NA150 and (b) NA100. The light gray shading represents nighttime.

evaporation results in an increase in N_a that is equal to the reduction in drop concentration. Collision-coalescence reduces N_c, thereby allowing for a cloud processing of the aerosol (reduction in N_a), albeit constrained by the assumed fixed lognormal shape. Surface precipitation removes drops from the atmosphere further enhancing the reduction in N_a. A constant surface aerosol particle flux of 70 cm^{-2} s^{-1}, estimated from Kazil et al. (2011), is applied for these long duration simulations in order to mitigate depletion of aerosol (Wang et al., 2010). Note that this prescribed surface aerosol flux is more than three times the value that one would have obtained with explicit use of the sea salt parameterization used in Clarke et al. (2006) and the wind speed from our simulations. Our preliminary tests with a range of surface sources suggested that using a smaller surface source moves the results toward a smaller initial N_a. This implies that the key results pertaining to the role of drizzle in the SCT to be shown below would be even stronger with smaller surface sources. Sedimentation is computed based on the bulk method of Morrison (2012) with the first-order upwind advection scheme.

The prognostic thermodynamic variables are liquid water static energy, mixing ratios of water vapor, cloud water (M_c), and rain water (M_r), supersaturation, number concentrations of aerosol (N_a), cloud droplets (N_c), and rain drops (N_r). Surface flux of momentum, temperature, and moisture are computed based on similarity theory. Radiation is computed every minute with the Rapid Radiative Transfer Model (RRTMG; Mlawer et al., 1997) with extended profiles above the domain top (4.25 km).

The domain size is 24 × 24 × 4.25 km^3, the horizontal grid spacing is 50 m, while the vertical grid spacing is 10 m below 2.775 km and stretched above. The time step is 3 s but an adaptive time step based on the Courant-Friedrichs-Levy stability criterion is used.

Four simulations are performed with different initial N_a specified over the entire domain: NA100 with 100 mg^{-1}, NA150 with 150 mg^{-1}, NA200 with 200 mg^{-1}, and NA250 with 250 mg^{-1}. (For reference, 1 mg^{-1} = 1 cm^{-3} at an air density of 1 kg m^{-3}.) A case based on NA100 but without rain production, i.e., without autoconversion and accretion, is also performed, and is referred to as NA100-NR. Note that NA100-NR does compute cloud droplet sedimentation.

Statistical output (one-dimensional time series and time series of profiles) are saved as hourly means, computed with 1 min sampling. Two-dimensional snapshot data (cloud water path, rain water path, etc.) are saved every 5 min. Three-dimensional snapshot data (prognostic variables) are saved every 3 h.

Yamaguchi et al. (2015) reported that NA150 exhibits a sensitivity of rain formation to horizontal domain size, with larger horizontal domains producing rain earlier. Figure 1 shows the time evolution of rain water path (L_r) simulated with four horizontal domain sizes (6 × 6 km^2, 9 × 9 km^2, 12 × 12 km^2, and 24 × 24 km^2) for NA150 (Figure 1a) and NA100 (Figure 1b). Yamaguchi et al. (2015) used simulations based on NA150 with the 12 × 12 km^2 domain for their analysis. For NA150, virtually no rain is produced for the smallest domain size (6 × 6 km^2), and the timing of rain generation is about a day earlier for the largest domain size (24 × 24 km^2). The results are similar for the two intermediate domain sizes. NA100 also exhibits its sensitivity to domain size; the effect is particularly large for the smallest domain. The differences between NA150 and NA100 derive from the initial N_a, as discussed below.

3. Results

3.1. SCT Accelerated by Drizzle

Renditions of the cloud field at 72 h for NA100-NR and NA100 are presented in Figures 2a and 2b. NA100-NR is in a cumulus under stratocumulus state while NA100 is in a precipitating cumulus state. Vertical profiles for NA100-NR (Figures 2c–2f) suggest that without rain formation NA100-NR follows the standard SCT theory, deepening and warming of the boundary layer, results in decoupling and the formation of a stable

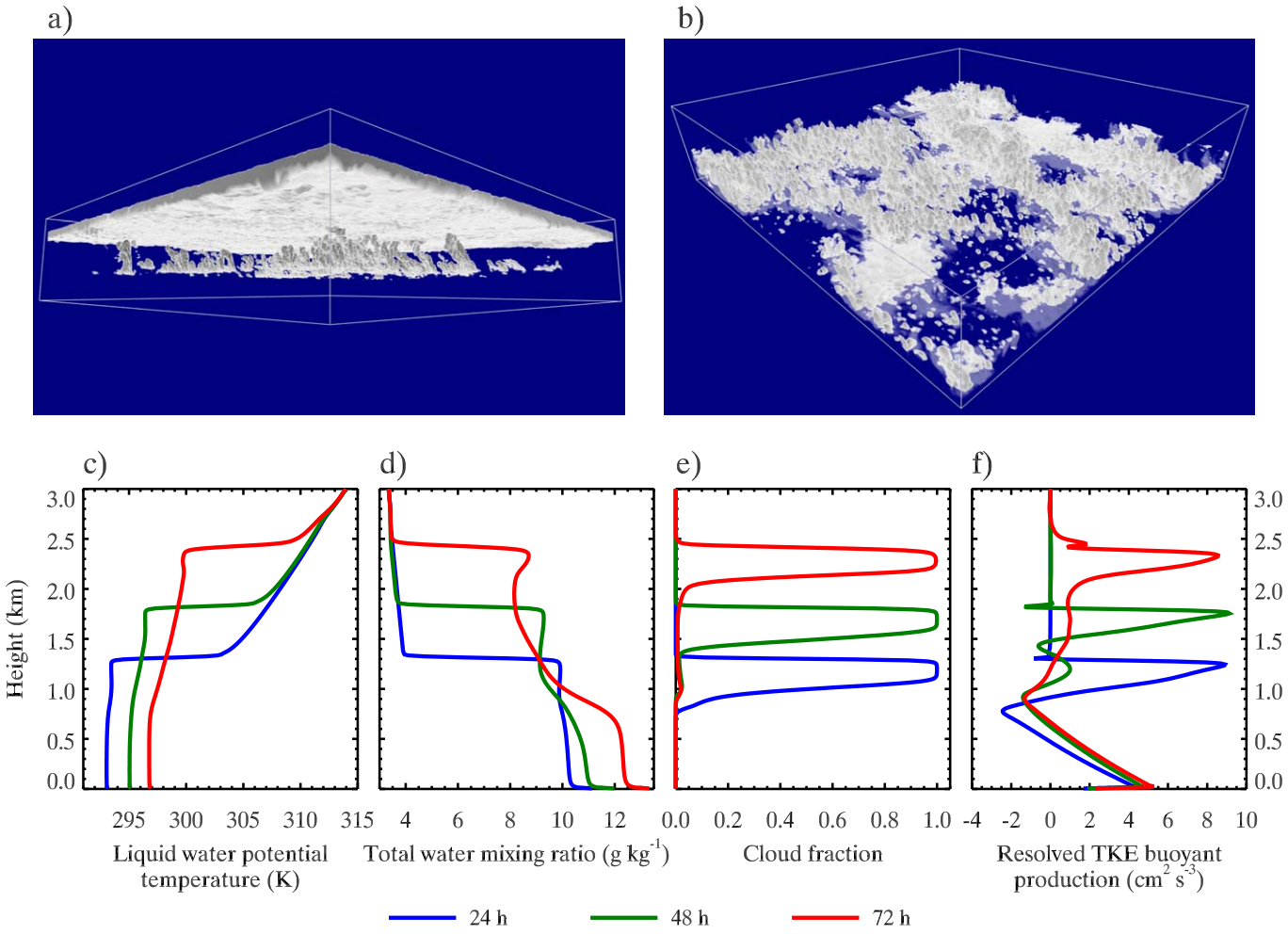

Figure 2. (a) A cloud field image at 72 h for NA100-NR and (b) for NA100. A translucent white color is used for rain water for NA100. (c–f) Hourly averaged vertical profiles of selected variables for NA100-NR every 24 h. Cloud fraction at each level is given as the number fraction of cloudy grids whose $M_c > 0.01$ g kg^{-1}.

layer above the cumulus cloud base. The upper stratocumulus layer gradually thins but maintains full cloud cover. (Cloud fraction at each level is computed as the number fraction of cloudy grids, using an M_c threshold of 0.01 g kg^{-1}.) The results are very similar to the CTLD case of BB14 (based on SS11, but performed with SAM), which produces minimal drizzle.

Figure 3 shows time series of cloud fraction, cloud water path (L_c), cloudy column average, cloud layer mean N_c, L_r, and inversion height (or PBL height) for all cases. Cloud fraction is defined based on a column cloud optical depth (in the visible) larger than 2. Inversion height is defined as the mean height of the largest vertical gradient of liquid water potential temperature.

The first feature of note is the regularity in the diurnal cycle of cloud fraction for NA100-NR (no rain), and prior to significant rain in the other cases. The second is the rising inversion height during the night. (The latter is consistent with CTLD of BB14 as well as SS11.) NA100-NR maintains an approximately constant N_c (mean $\approx$ 133 cm^{-3}, standard deviation $\approx$ 10 cm^{-3}). For all cases, N_c becomes larger than the initial N_a as a result of transport of aerosol from the subcloud layer into the stratocumulus layer. Due to the presence of decoupling (except during the first night), the aerosol supply from the subcloud layer is inefficient, so that N_a in the subcloud layer accumulates as time evolves (see Figure 4h for NA100, between 12 and 36 h, prior to rain).

Prior to the transition, there are minor differences in L_c among the cases during the first night (10–20 h); smaller initial N_a (i.e., smaller N_c and larger drops) results in larger L_c and a slightly shallower PBL height

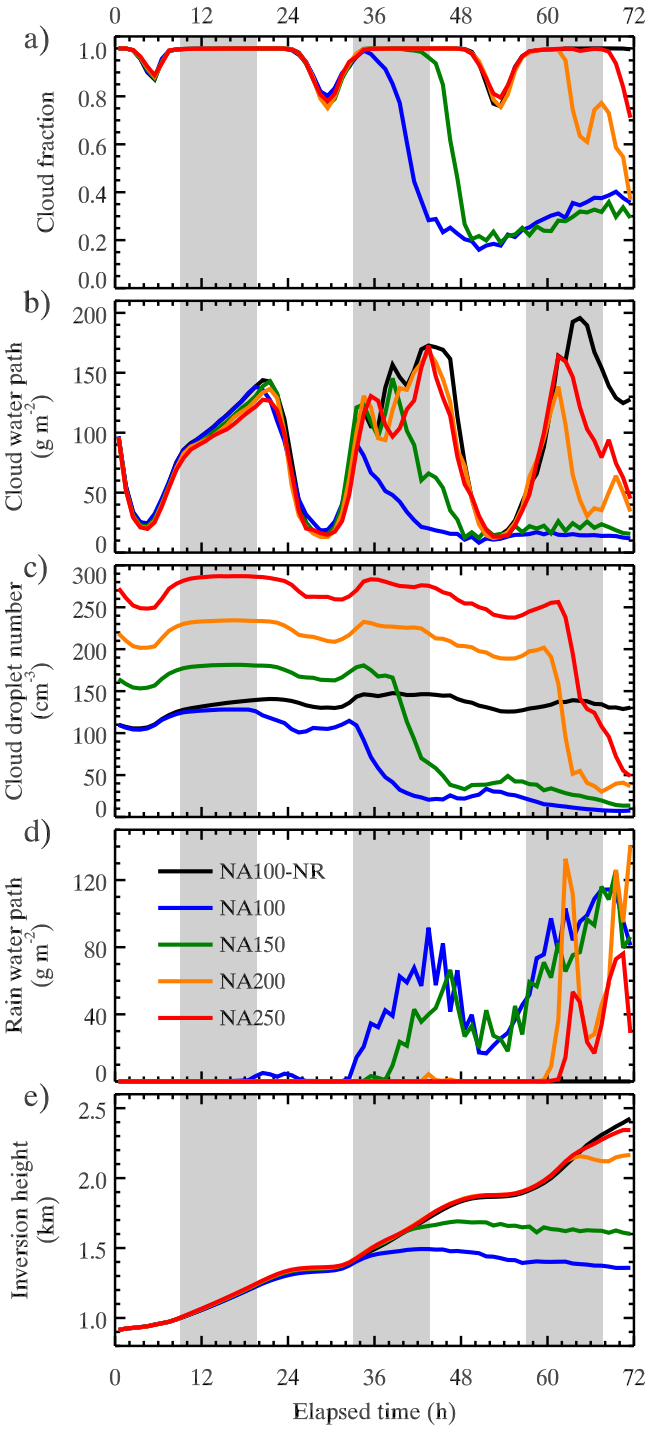

Figure 3. Time series of selected hourly averaged variables for the five cases. Domain mean L_c and L_r are shown. Cloud fraction is given as the number fraction of cloudy columns whose visible optical depth exceeds 2. Cloud droplet number is the cloud layer mean N_c over cloudy columns, and cloud base and top are the lowest and highest levels with an M_c threshold of 0.01 g kg^{-1}. Inversion height is the mean height of the maximum vertical gradient liquid water potential temperature.

(Figures 3b and 3e). Our analysis is consistent with Bretherton et al. (2007), who showed the influence of cloud droplet sedimentation on entrainment efficiency and thus L_c; by suppressing entrainment, the faster drop terminal velocities associated with larger drops (lower N_a) result in larger L_c. (See also de Lozar & Mellado, 2016, who recently studied the sedimentation effect on entrainment velocity using direct numerical simulation.)

For the cases that do generate precipitation, there is a distinct departure from the diurnal cycle, the onset of which is inversely proportional to the initial N_a; cloud fraction decreases rapidly within a period of approximately 8–10 h, accompanied by sharp decreases in L_c and N_c, and rapid production of L_r. Drizzle is thus responsible for this fast transition to a low cloud fraction state. Once this rapid transition is initiated, the PBL height remains almost steady, albeit with a slowly lowering trend. For NA100, the small L_r that develops between 18 and 26 h is insufficient to modify the diurnal cycle, or to cause divergence from the standard SCT theory. The time series of N_c exhibit an interesting feature; the rate of reduction in N_c becomes steeper with increasing N_a. At high N_a aerosol suppresses collision-coalescence, but when sufficient cloud water accumulates the cloud water becomes colloidally unstable and rapidly transitions to rain. At smaller N_a, rain is more prevalent so that L_c does not build up as much, and the rate of reduction in N_c is more gradual. Similar threshold behavior was discussed in Feingold et al. (2013).

The cumulus state shown in Figure 2b for NA100 appears after the rapid transition initiated by precipitation. Profiles of selected variables for NA100 are shown every 12 h in Figure 4. Because NA150, NA200, and NA250 follow the same transition pattern to NA100, albeit with delay, we do not show their profiles. Precipitation flux (Figure 4i) is the net sedimentation flux of cloud and rain water, and latent heating (Figure 4j) is calculated from the divergence of the precipitation flux. Consistent with Figure 3, there is a clear transition from a stratocumulus state to a cumulus state, which occurs during the second night (near 36 h). Before 36 h, the evolution follows SCT theory, and a cumulus under stratocumulus state emerges. Large drizzle drops (i.e., rain water, Figure 4e) form in the cloud layer at 24 h, and evaporate near the cloud base (Figure 4i). As seen in Figure 3, this weak drizzle does not modulate the transition (in accord with SCT theory), and its effect is limited by subsequent cloud thinning due to solar heating that suppresses the cloud water, and therefore drizzle. Later, rain precipitates below cloud base (at about 36 h) and reaches the surface in more significant amounts by 48 h. At 48 h, the PBL has transformed into a cumulus field; it becomes poorly mixed and stable above ~200 m (inset of Figure 4a) and cloud fraction is reduced to less than 0.2. Domain mean M_c and cloud mean N_c are substantially reduced (Figures 4d and 4f). This relatively rapid transformation into a cumulus state by drizzle is not predicted by the SCT theory.

The influence of drizzle/rain on the structure of the PBL appears in many ways. At 36 h, while stratocumulus still exists, the buoyant production of resolved scale TKE near cloud base becomes positive (Figure 4k). This is caused by destabilization via evaporative cooling of drizzle (Figure 4j) that is concentrated at the cloud base (Jiang et al., 2002); the cooler cloud base conditions are more favorable for convection. At 48 h, drizzle shapes a thermodynamically stable cumulus cloud layer via the latent warming associated with rain formation, and a stable subcloud layer via the latent cooling of rain evaporation (Figure 4j), except below ~200 m where it is thermodynamically unstable (Figure 4a). A stable layer above an unstable

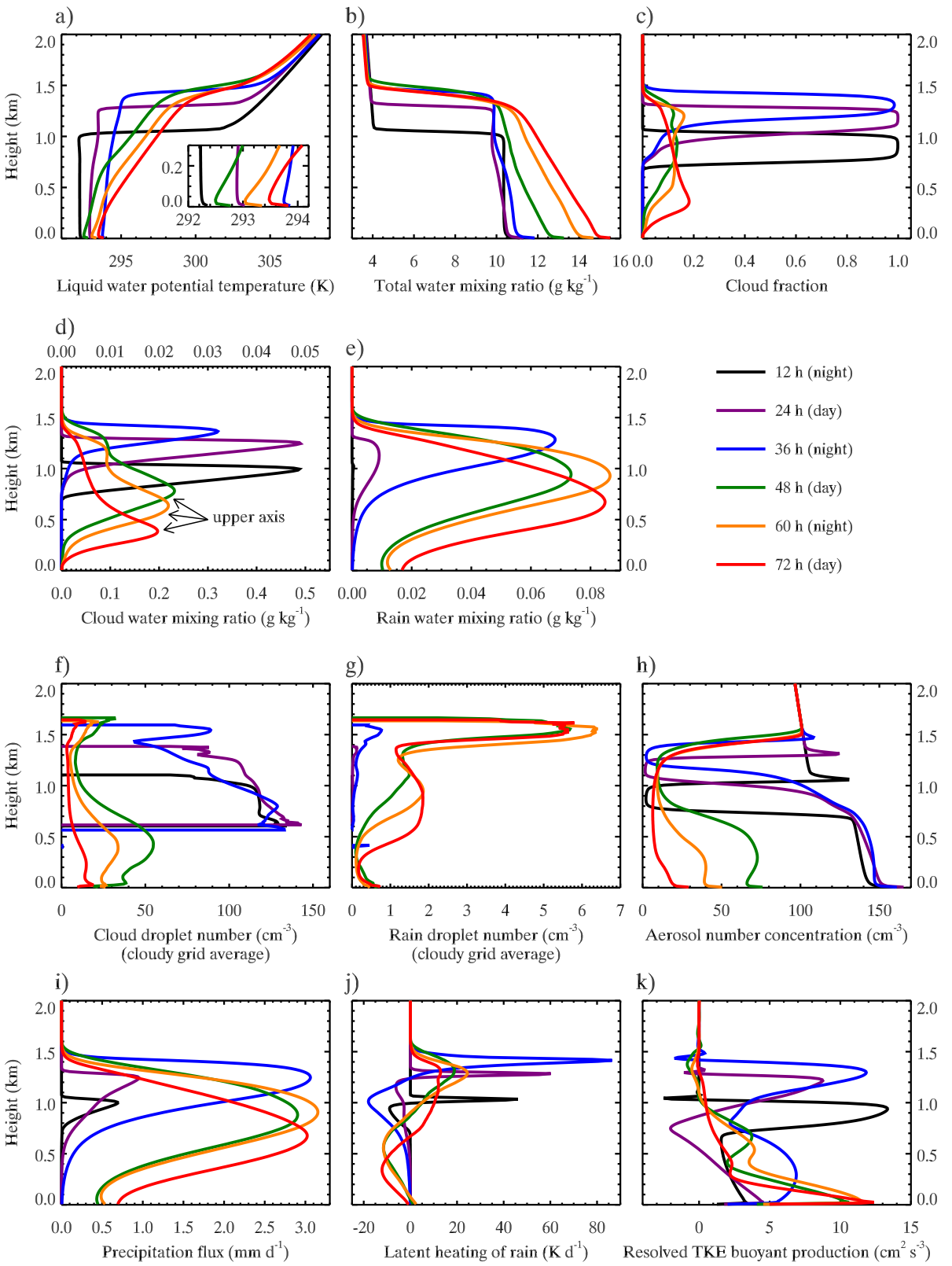

Figure 4. Vertical profiles of selected hourly averaged variables for NA100 every 12 h. A dual horizontal axis is used for (d) M_c; the upper axis is for 48, 60, and 72 h. Precipitation flux is the net sedimentation flux of cloud and rain water, and latent heating is associated with the flux divergence of precipitation.

surface layer already exists at 36 h. This follows PL91's prediction for a temperature profile influenced by drizzle. The evaporation of precipitation results in destabilization near the surface, which increases surface buoyant production of TKE (Figure 4k; cf., Figure 2f). During the stratocumulus state, SS11 noted stabilization via evaporative cooling of weak drizzle extending throughout the subcloud layer, which weakens convection and leads to decoupling. This stabilization effect exists at 24 h in our simulation (Figures 4a, 4j, and 4k).

Compared with the temperature at the lowest level for NA100-NR, which warms from 292 to 297 K over 72 h, for NA100, it remains cooler than 294 K at all times (Figure 4a) due to rain evaporation. Since SST increases progressively, surface sensible heat flux increases rapidly ($\approx$ 9 W m^{-2} at 36 h, $\approx$ 26 W m^{-2} at 48 h, and $\approx$ 33 W m^{-2} at 72 h). The increased surface sensible heat flux counteracts the subcloud layer cooling by rain, and imposes a net warming in the subcloud layer (Figure 4a between 48 and 72 h). This warming trend might lead to reformation of a mixed subcloud layer above which shallow cumulus typically grow (cf., Figure 2c for NA100-NR). In contrast, NA100-NR maintains a mixed subcloud layer, progressively warming the lowest level to 295 K at 48 h and 297 K at 72 h (Figure 2c), while maintaining a negative cloud base buoyant production of TKE (Figure 2f), and a near constant surface sensible heat flux of $\approx$ 7 W m^{-2}.

Consistent with PL91, this mostly stable cumulus PBL for NA100 forms a moist subcloud layer (Figure 4b; cf., Figure 2d) due to limited moisture transport into the cloud layer by cumuli, and results in a nearly steady surface latent heat flux of $\approx$ 121 W m^{-2}. (NA100-NR has $\approx$ 116 W m^{-2} at 36 h, $\approx$ 141 W m^{-2} at 48 h, and $\approx$ 166 W m^{-2} at 72 h.) As a result, cloud base becomes progressively lower; the domain mean relative humidity at the lowest level progressively increases to $\approx$ 0.71 at 36 h, $\approx$ 0.85 at 48 h, $\approx$ 0.91 at 60 h, and $\approx$ 0.93 at 72 h. (NA100-NR maintains a domain mean relative humidity at $\approx$ 0.67.) Lastly, the shape of the cloud fraction profile changes from a top heavy shape at 36 h to a bottom heavy profile, which is similar to the profile of precipitating cumulus (vanZanten et al., 2011).

3.2. Drizzle Formation in Cumulus

Although stratocumulus drizzle was predicted by PL91 as a triggering mechanism for the SCT, in the current study initiation of precipitation that triggers stratocumulus breakup is identified in the penetrative cumulus rather than in the stratocumulus deck.

Figures 5 and 6 show selected two-dimensional variables at 30 and 33 h for NA100. According to Figure 3, nonprecipitating stratocumulus has started redeveloping at 30 h, but by 33 h L_r has increased noticeably. These figures include a measure of decoupling, Δz_b, defined by Jones et al. (2011) as

$$\Delta z_b = z_b - z_{\mathrm{LCL}}\,, \tag{1}$$

where z_b is cloud base height and z_{LCL} is the lifted condensation level (LCL). z_b is diagnosed as the lowest level with an M_c threshold of 0.01 g kg^{-1}, and z_{LCL} is calculated iteratively by adiabatically raising an air parcel from the surface. Large positive values indicate a strongly decoupled column while negative values indicate an unstable column since in this case cloud would form below the estimated LCL. For each column, PBL mean vertical wind velocity and PBL integrated water vapor are computed below the inversion height.

At 30 h, clouds are distributed inhomogeneously; a cluster with large L_c develops within the black circle. This cloud cluster comprises penetrating cumulus characterized by larger cloud depths, less decoupling, stronger convection (stronger updrafts associated with cumulus clouds in the circle), and moister air than other regions. For these cumulus, Δz_b is expected to be smaller, i.e., less decoupled, because the cumulus cloud base is closer to the z_{LCL}. At 33 h, a cluster with high L_r appears. This precipitating cluster is characterized by similar properties to the cloud cluster at 30 h and is a more evolved state of the cloud cluster at 30 h.

Figure 7 shows a cross section at $y = 11$ km (cf., Figure 6) at 33 h for M_c, M_r, rain drop geometric-mean radius ($r_{g,r}$), and vertical velocity squared (w'^2). The perturbation wind field (i.e., turbulence) is superimposed on the w'^2 contours. For this figure, both M_r and N_r are filtered with an M_r threshold of 0.001 g kg^{-1} and an N_r threshold of 0.015 cm^{-3} for a minimum $r_{g,r}$ of approximately 25 μm. The M_r threshold is one order of magnitude smaller than our M_c threshold.

The cross sections of M_c and M_r (Figures 7a and 7b) show nonprecipitating and precipitating regions. The nonprecipitating region (approximately $x < 8$ km and $x > 17$ km) has moderate M_c (generally less than 0.8 g kg^{-1}), cloud layer thickness less than approximately 300 m, and weak turbulence, which are all signatures

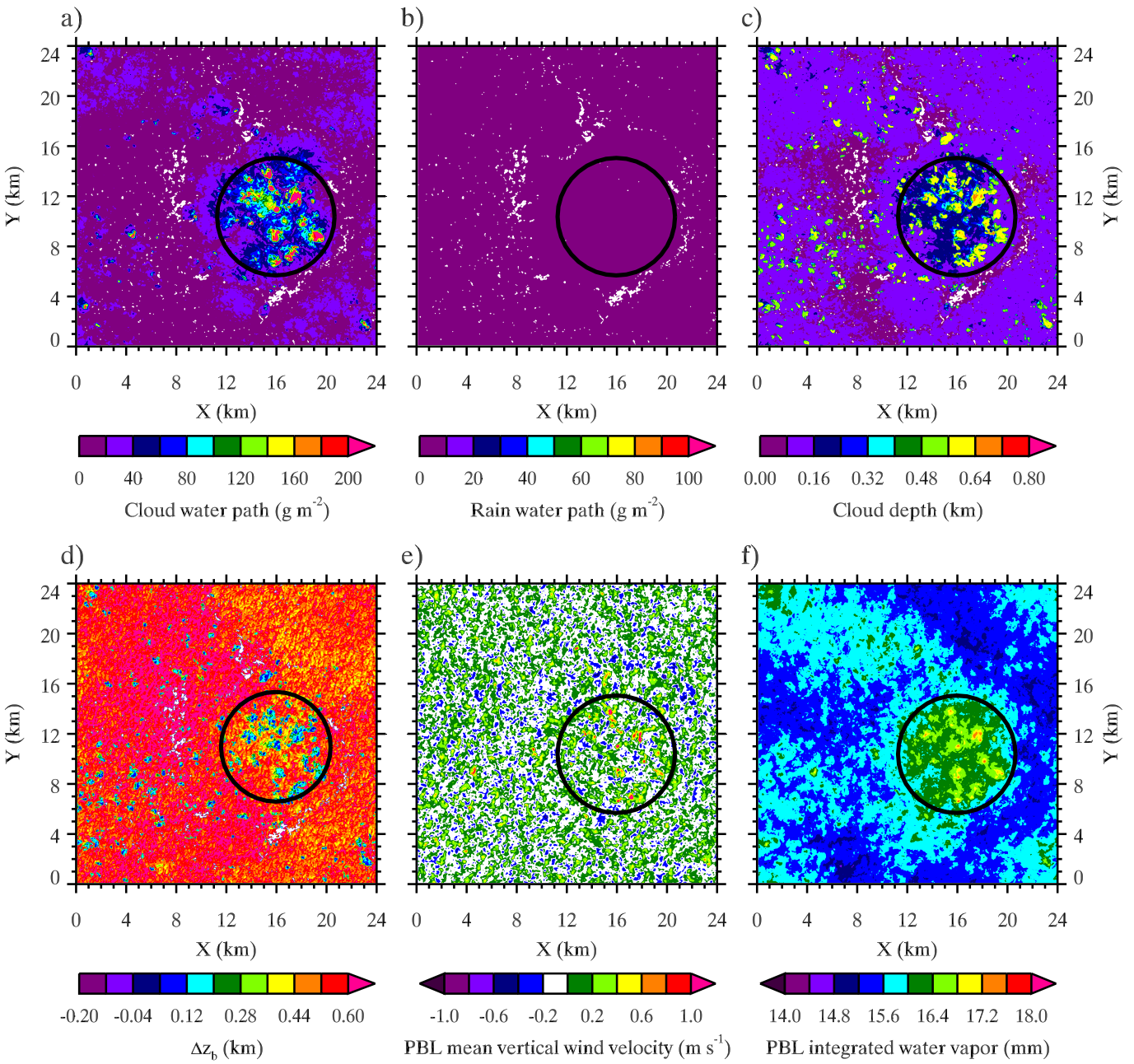

Figure 5. Selected two-dimensional variables for NA100 at 30 h. In order to show the region of interest near the domain center in this figure as well as Figure 6, the domain is shifted by 12 km in both directions.

of stratocumulus. In the precipitating region (approximately 8 km $< x <$ 17 km), a drizzle shaft exists between two penetrative cumulus located at ~9.5 km and ~13 km, both of which have stronger convection/turbulence and stronger updrafts than their surroundings. For these cumulus, both M_r and $r_{g,r}$ are smaller than those in the drizzle shaft, which means that precipitation in the cumulus is at a relatively early stage of rain drop growth, compared to the mature drizzle shaft. A circulation pattern in the turbulent wind field between the two cumulus suggests that collision-coalescence growth within the recirculation zone might play an important role in precipitation formation (e.g., Rauber et al., 1991). The latter study showed that raindrops grow preferentially as they recirculate within eddies along updraft/downdraft shear zones.

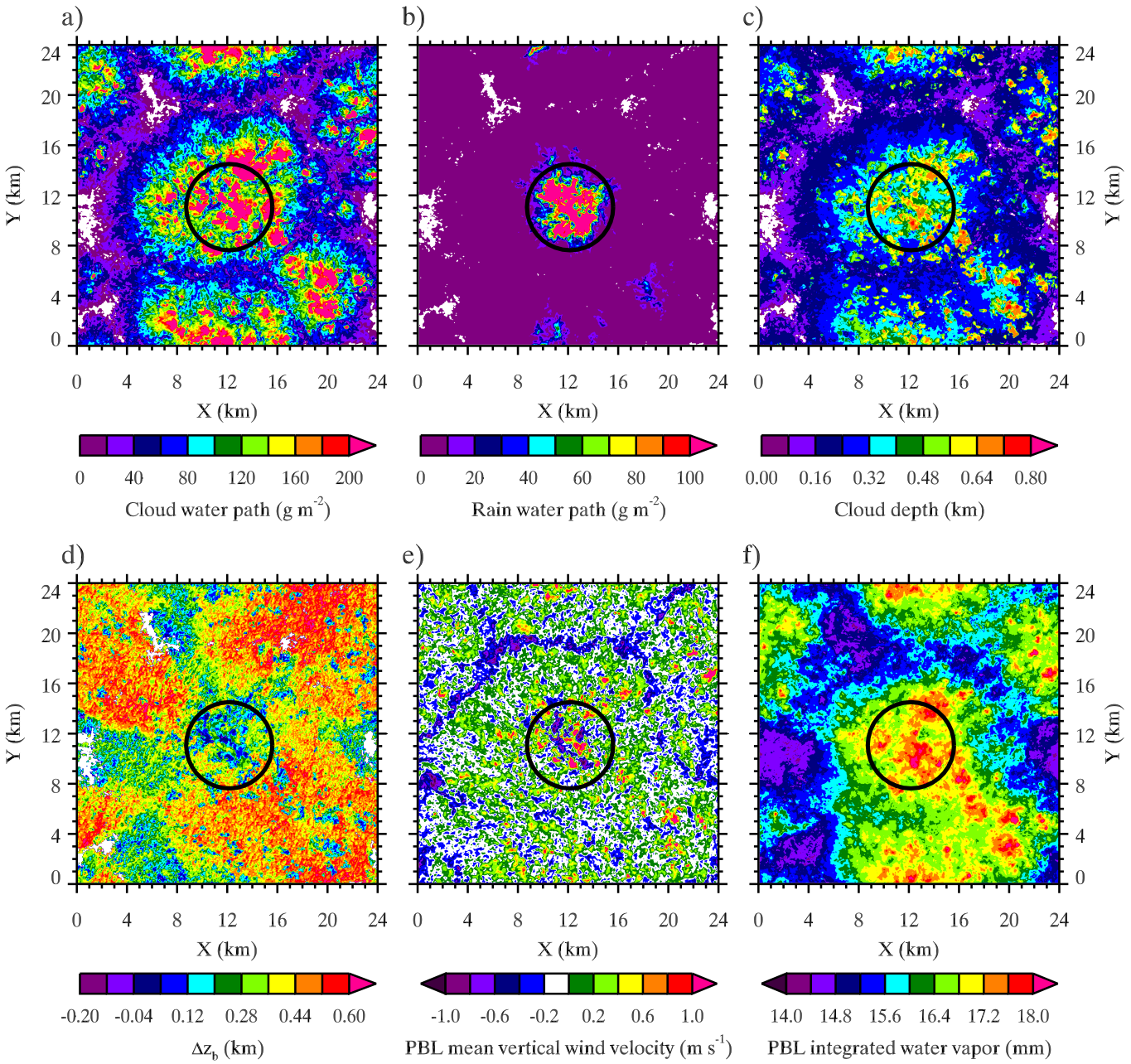

Figure 6. As in Figure 5 but at 33 h.

From this analysis, it is clear that the drizzle in the precipitating cluster shown in Figure 6 is not rooted in the stratocumulus layer but rather in the penetrating cumulus. The supply of drizzle drops from the penetrative cumulus to the stratocumulus enhances drizzle droplet growth and triggers strong precipitation which promotes stratocumulus breakup. Visual inspection shows that another large drizzle region between 13.5 and 14.5 km develops into a drizzle shaft later.

Theoretically the formation of drizzle in deepening cumulus is expected; rain rate R scales as

$$R \sim L_c^{\alpha} N_c^{-\beta}, \tag{2}$$

(e.g., Comstock et al., 2004; Feingold et al., 2013; Feingold & Siebert, 2009; Pawlowska & Brenguier, 2003; vanZanten et al., 2005). Feingold and Siebert (2009) estimated that $\alpha \sim 2.4\beta$ with $\alpha \sim 1.6$ and $\beta \sim 0.67$ for

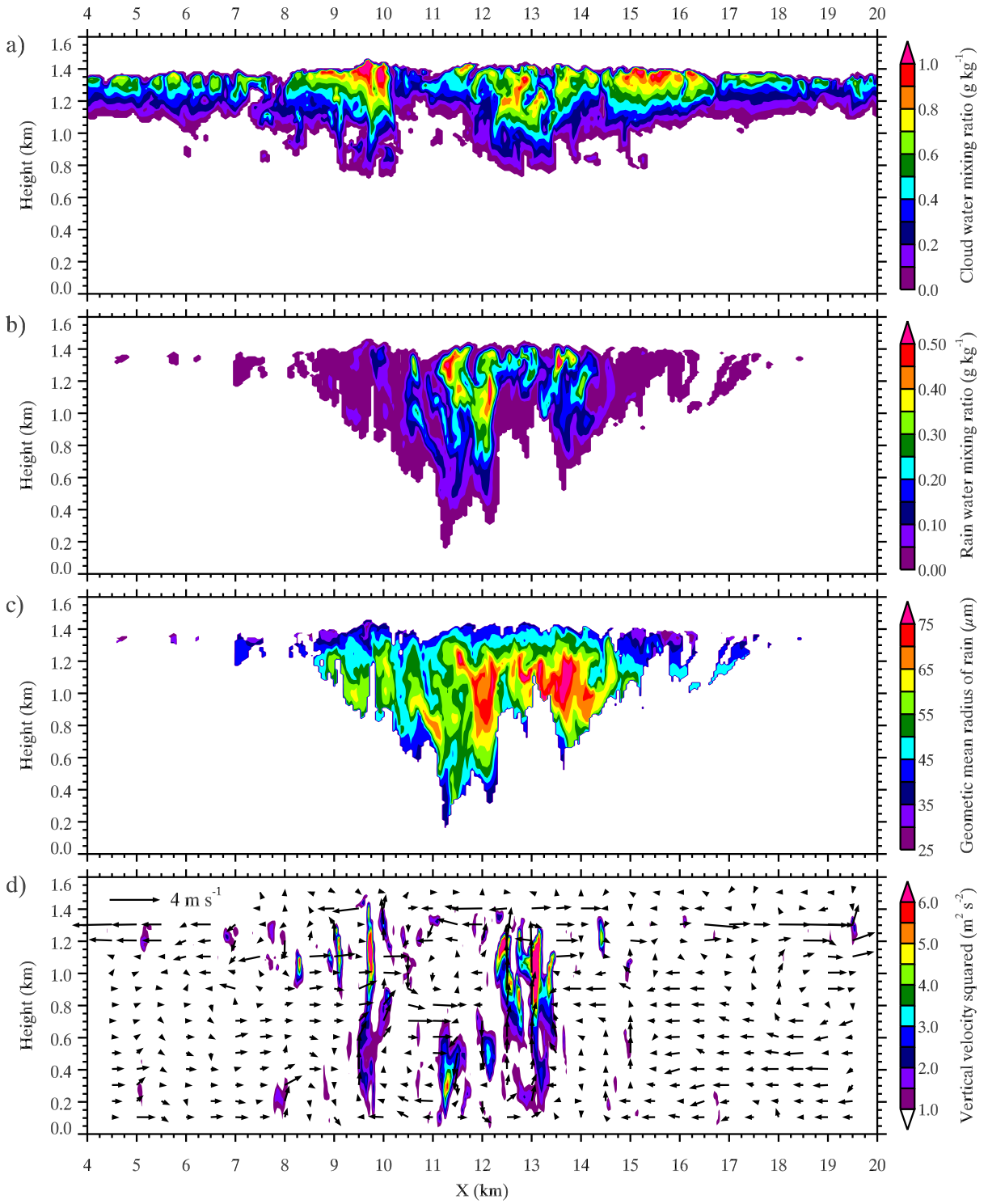

Figure 7. Cross section at $y = 11$ km between $x = 4$ and 20 km at 33 h. The cross section is extracted after the horizontal data domain has been shifted by 12 km in both x and y directions in order to match Figure 6. M_r in (b) and N_r are filtered with two conditions: an M_r threshold of 0.001 g kg^{-1} and an N_r threshold of 0.015 cm^{-3} so that the smallest $r_{g,r}$ is 25 μm. $r_{g,r}$ in (c) is computed with the filtered M_r and N_r. In (d), the perturbation wind field is superimposed on the w'^2 field.

stratocumulus so that deepening (higher L_c) has a stronger influence on R than does N_c. For each of our simulations, increases in L_c are the primary driver for substantial increases in R since N_c is approximately constant (e.g., for NA100, the mean N_c is $\approx$ 116 cm^{-3} and the standard deviation is $\approx$ 17 cm^{-3} for cloud-

averaged N_c for the first 33 h computed from the three-dimensional snapshot data), and only the penetrative cumulus can achieve large L_c because they are much deeper than the stratocumulus above. (Under adiabatic conditions, $L_c \propto H^2$ where H is cloud depth.)

3.3. Runaway Feedback and Changes in Cloud Field Morphology

N_c and N_a are reduced significantly through both collision-coalescence scavenging and wet deposition, further enhancing the conversion of cloud water to rain water (Figures 4f and 4g). For the current configuration, vertical transport of aerosol via entrainment, as well as the prescribed surface source to the cloud layer, is incapable of slowing down the feedback. Analysis shows that entrainment is not sufficiently effective at transporting aerosol from the free atmosphere to the boundary layer in amounts that would suppress precipitation formation.

Drizzle initially formed in the cumulus clouds becomes strong enough to promote a precipitation-generated spatiotemporal rearrangement or "oscillation" in the cloud structure, which is also characteristic of open cellular convection (Feingold et al., 2010; Wang et al., 1993; Wang & Feingold, 2009; Yamaguchi & Feingold, 2015). In the aforementioned studies, precipitation generates surface divergence patterns, followed by the formation of new cumulus at the convergence of the surface outflows, which later become locations of divergence when substantial precipitation develops. In Figure 7d (at 33 h), drizzle emanating from the heavy drizzle shaft approaches the surface, creates turbulence via evaporation, and generates surface divergence. A broader view can be seen in Figure 8, which shows a time series of the oscillation associated with surface divergence observed in L_c, L_r, and surface rain rate (R_{sfc}) for NA100. The Hovmöller diagrams, created by averaging over the y direction, show that the periodic appearance of packets of high values for all variables, and the small temporal scale fluctuations in the domain mean time series are well correlated with the appearance and disappearance of the packets. This is consistent with Feingold et al. (2010) who showed Hovmöller diagrams with symmetrical propagation/rearrangement of packets in both westward and eastward directions when the simulation was initialized with no mean wind. For the current simulations, with an easterly mean zonal wind, the packets of intense values have a major westward propagation and a secondary eastward propagation.

The observed drizzle-induced oscillation is likely biased by the domain size. First, the size of the packet of drizzle that triggers the transition is roughly 6–8 km, which occupies about 10% of the area (Figure 8b). The size of the stratocumulus cell containing that drizzle is ~25% of the domain size (Figure 6a). Thus, the domain size is admittedly too small. This artificially increases the frequency of the oscillation, which may influence the timeframe for the transition.

The SCT induced by cumulus precipitation will not take place when the PBL has access to ample aerosol in the boundary layer (e.g., McGibbon & Bretherton, 2017, hereafter MB17) or free atmosphere during the stratocumulus state (Yamaguchi et al., 2015). MB17 estimated N_c from observations and applied it to all cloudy grids in their simulations. With values of N_c on the order of 90–50 cm^{-3} during the transition phase their simulations did not generate sufficient precipitation to trigger the SCT. With simulations based on the SS11 SCT case, Yamaguchi et al. (2015) show the formation of a thicker, nonprecipitating stratocumulus layer when biomass burning smoke is entrained into the stratocumulus state and shuts off drizzle production. The SCT initiated by cumulus drizzle may also slow down or be terminated when significant concentrations of aerosol are imposed, even after the transition has initiated. Feingold et al. (2015) discuss the transition from open cellular circulation to closed cellular circulation as a result of increasing N_c.

Our simulations show that free tropospheric and surface aerosol sources are insufficient to slow the drizzle-induced SCT significantly, in part because they are not efficiently mixed into the clouds. The question arises as to whether a more significant aerosol source, readily accessible to the cloud, would be able to do so. Such a source might result from large-scale advection of aerosol into the region. To this end, an additional test was performed for NA100 but with a prescribed volume aerosol source instead of the specified surface aerosol source of 70 cm^{-2} s^{-1}. The volume aerosol source is intended to represent surface sources, advection of aerosol into the domain, and new particle formation (plus subsequent growth to cloud condensation nucleus sizes). A source strength is set to 2.5 mg^{-1} h^{-1}, which is equivalent to instantly, homogeneously distributing an aerosol source of 70 cm^{-2} s^{-1} over a 1 km depth. The volume source is applied at all grid points. After the PBL grows deeper than 1 km, which occurs around 9 h, the source strength directly applied to the PBL becomes larger than the surface source specified in the standard set of simulations. Figure 9

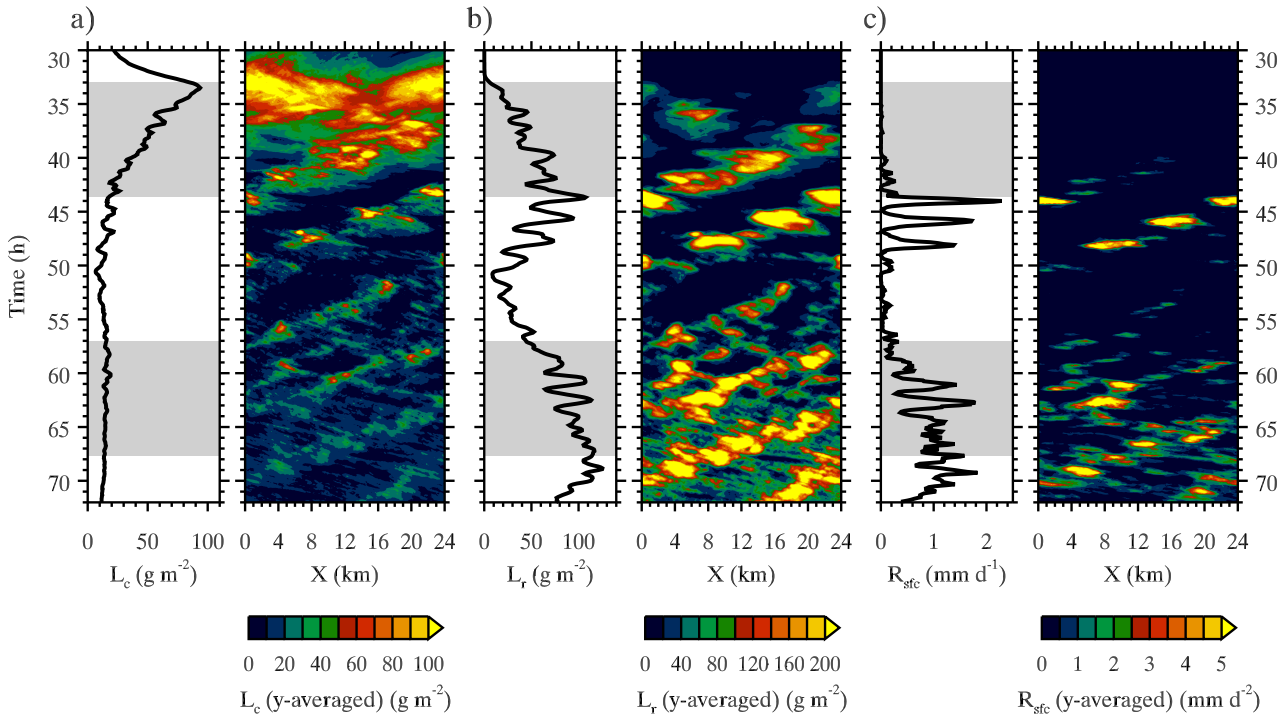

Figure 8. Time evolution of (a) L_c, (b) L_r, and (c) R_{sfc} for NA100 from 30 h onward. For each variable, the line plot shows the time evolution of the domain mean, and the contour plot shows the Hovmöller diagram created with a *y*-directional average. Data points are 5 min apart.

shows that for this enhanced source strength, the evolution of cloud and PBL fields is similar to NA150, i.e., the volume source delays transition compared with NA100. Thus, our results are qualitatively independent of the representation of the aerosol replenishment; even a large volume source results in drizzle-induced SCT. One notable effect of the volume source is that cloud fraction (defined by visible cloud optical depth greater than 2; solid line) recovers at around 52 h (Figure 9a). Further examination shows that during this time, optically thin stratocumulus is formed; this is deduced from the fact that when a cloud optical depth of 5 is used as a threshold, the cloud fractions are similar.

4. Simulations With Fixed Droplet Number Concentration

Traditionally, precipitation has been thought to play a minor role in the SCT. This is because drizzle produced in the stratocumulus deck is too weak to modulate the SCT (W97; SS11), and simulated cloud fraction remains high in the presence of rain in the penetrative cumulus (W97). On the other hand, our simulations show that precipitation forming in penetrative cumulus does reshape and accelerate the evolution of the SCT. Even with an initial $N_a = 250$ mg^{-1}, drizzle breaks up the stratocumulus deck rapidly for the case studied here.

One possible explanation for this difference is our use of a more advanced microphysics parameterization, which predicts concentrations of aerosol and drop number concentrations, and therefore allows them to fluctuate more naturally. The bin-emulating two-moment scheme keeps a budget on aerosol and cloud number mixing ratios. It accounts for activation of aerosol particles based on ambient supersaturation, condensation, evaporation and the concomitant regeneration of aerosol particles, and the removal of aerosol by surface precipitation. W97 used a one-moment bulk scheme, and SS11 used a two-moment bulk scheme with fixed N_c. The SCT intercomparison study (de Roode et al., 2016) also used a fixed N_c. SS11 reduced N_c to one third of their nominal value (100 cm^{-3}) to increase drizzle for their precipitation case. For this relatively small N_c of 33 cm^{-3} compared with those in the current study, SS11 saw a faster decrease in cloud fraction relative to their base case but did not see significant changes in other parameters (e.g., L_c, latent and sensible heat fluxes; PBL height is a little lower but grows continuously). This led the authors to

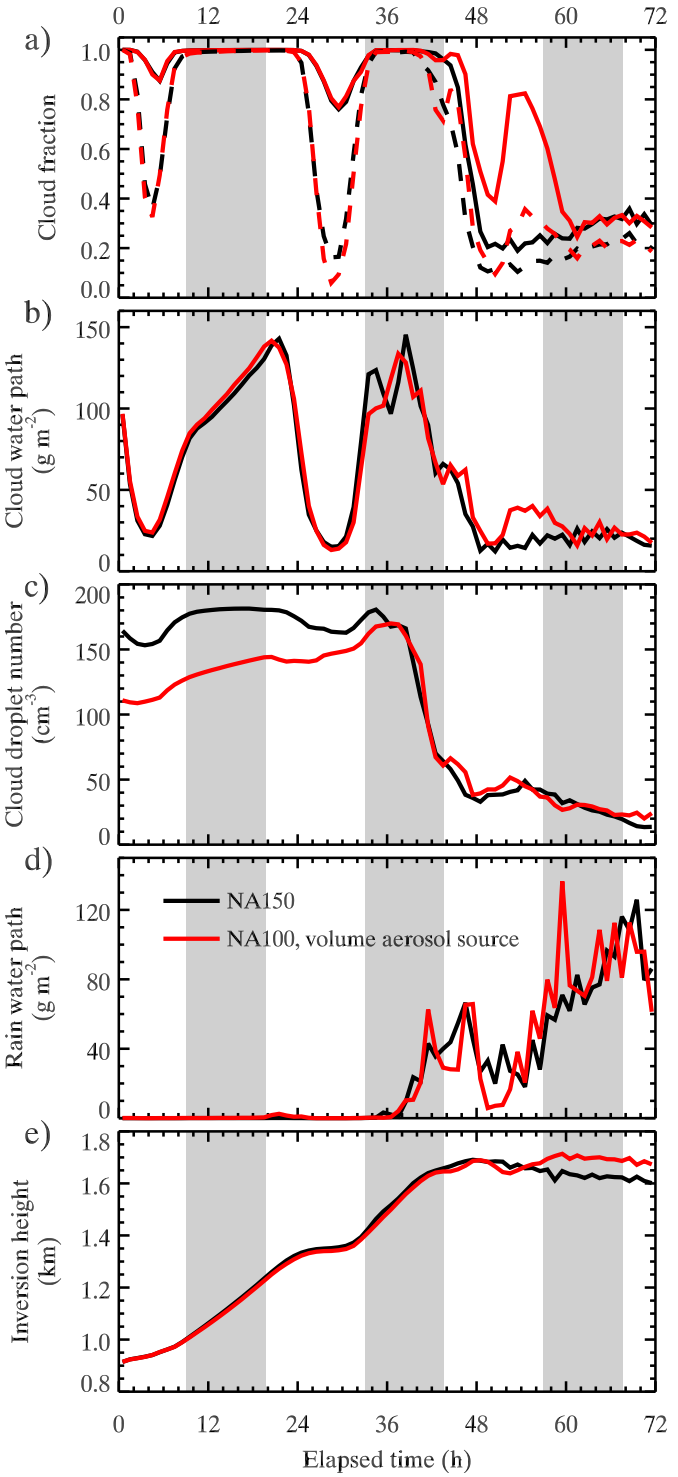

Figure 9. Same as Figure 3 but for NA150 and NA100 with a volume aerosol source of 2.5 mg^{-1} h^{-1}. The cloud fraction time series drawn with the dashed line is diagnosed with visible optical depth larger than 5.

conclude that the basic evolution of the SCT is not affected by precipitation. It should be noted that with an initial N_a of 50 cm^{-3}, our model results in transition within the first day. As noted above, MB17 elaborated upon the fixed N_c approach and applied a time-varying, observationally derived N_c (roughly 90–50 cm^{-3}) whenever condensate occurred. MB17 tested the influence of drizzle with a fixed $N_c = 50$ cm^{-3}, which slightly increased precipitation, but found that the differences from their reference case simulated with a prescribed time varying N_c were minor. These studies did not allow a natural evolution of the aerosol through collision-coalescence and surface precipitation, which constitutes a positive feedback, the rate of which is commensurate with the rain process itself. This might be particularly important in pockets of high liquid water content, where the combination of high M_c (and M_r) and low N_c would tend to rapidly accelerate drizzle formation, e.g., equation (2). Moreover, by applying N_c wherever condensate occurs, they assume that the aerosol can be transported to the cloud in a poorly (or locally) coupled boundary layer.

Another factor to consider is the larger horizontal domain size used in this study. (In SS11 the maximum domain size was 8.96 × 8.96 km^2 and in MB17 it was 6.4 × 6.4 km^2.) As mentioned above, we see an influence of domain size on the timing of rain formation; a larger domain produces rain earlier. Kazil et al. (2017) find higher L_c and a wider probability distribution function with more frequent peak L_c on larger domains. Similar sensitivities of the L_c probability distribution function to domain size were reported by Yamaguchi et al. (2013). Locally high L_c on larger domains will give rise to faster collision-coalescence and more rapid drizzle and rain formation. The influence of this rain will tend to spread through the domain via cold pool formation and convergence.

A number of potential biases should be considered when assessing the robustness of the results presented herein vis-à-vis domain size. First, larger domains will generate a tail of high liquid water path and therefore more rain. Second, once the rain starts, smaller domains will experience a larger degree of clustering because of the doubly periodic boundary conditions, which will accelerate rain. These two factors therefore compensate to some extent. One finds support for this compensation in Figure 1b where one notes that the timing of rain formation for the 9, 12, and 24 km domains is very similar.

Further perspective comes from considering different scalar advection schemes and their potential influence on the formation of rain. BB14 used the second-order monotonic advection scheme of Smolarkiewicz and Grabowski (1990) for their CTLD case, and noted an increase in L_c when using a higher-order scalar advection scheme. (Note that BB14's CTLD and our NA100 differ in microphysics scheme, scalar advection scheme, and domain size.)

To explore these ideas, additional simulations are performed with fixed N_c using the microphysics scheme of Khairoutdinov and Kogan (2000, hereafter KK00) and for domain sizes of 6 × 6 km^2, 12 × 12 km^2, and 24 × 24 km^2 (the domain size used in all simulations herein). The specified N_c is 100 cm^{-3}, following SS11's control case. Cloud water sedimentation is simulated based on the parameterization of Ackerman et al. (2009). To investigate the impact of the scalar advection scheme, one additional simulation is performed with the second-order MPDATA scheme, but is otherwise the same as NA100 (NA100-MPDATA).

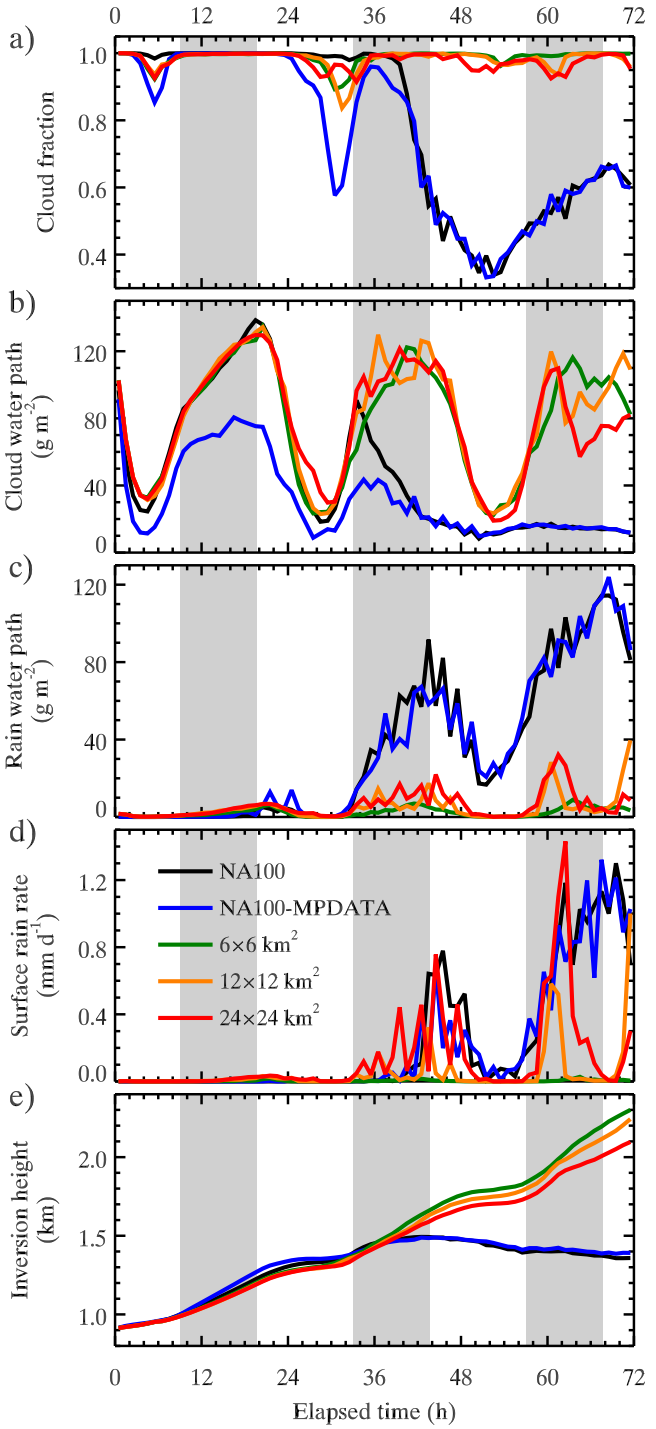

Figure 10. As in Figure 3 but for NA100 (black), NA100-MPDATA (i.e., simulation as in NA100 but with a second-order scalar advection scheme; blue), and simulations with the KK00 microphysics scheme with fixed N_c for various domain sizes (green, orange, and red). R_{sfc} is also shown. Cloud fraction in this figure is not defined by optical depth, but using M_c greater than 0.01 g kg^{-1}, since the KK00 scheme does not define the cloud droplet size distribution, which would be required to compute optical depth.

Figure 10 shows selected time series of fields from the simulations with the KK00 scheme for the three different domain sizes (green, orange, and red), as well as NA100-MPDATA (blue) and NA100 (black), which both employ the two-moment microphysics scheme. As discussed above, NA100 produces enough drizzle to accelerate the SCT with $N_c \approx 116$ cm^{-3}. NA100-MPDATA produces smaller L_c during the period in which stratocumulus exists (prior to cloud fraction becoming small), and generally a higher inversion height, but captures the timing of the transition, L_r, and R_{sfc} very well. For the KK00 simulations, there is weak sensitivity to domain size; a larger domain produces marginally more drizzle. As much precipitation reaches the surface as in NA100 for the largest domain size (24 × 24 km^2) between 36 and 50 h, however it does not accelerate the transition as in the case of NA100 because the conversion from cloud water to drizzle does not experience the positive feedback described above due to fixed N_c. Consistent with MB17, a further test with the KK00 scheme with $N_c = 50$ cm^{-3} for the 6 × 6 km^2 domain is comparable to the case with $N_c = 100$ cm^{-3} for the 6 × 6 km^2 domain, with some minor differences. Apparently, the lack of a positive feedback in the KK00 simulations also strongly weakens the sensitivity of rain to domain size (cf., Figure 1). The inference is that for weak drizzle, the offsetting biases associated with domain size and periodic boundary conditions are small.

5. Summary

In this study, we have investigated the role of precipitation in the stratocumulus to cumulus transition (SCT) using large eddy simulations with a bulk two-moment microphysics scheme that predicts number concentrations of cloud and rain drops, and aerosol. Simulations are initiated with moderate aerosol number concentrations (100–250 cm^{-3}), which produce little to no drizzle from the simulated stratocumulus clouds. Contrary to past modeling studies, all simulations exhibit an abrupt transition to a cumulus state over a period of approximately 10 h once drizzle forms in sufficiently deep cumulus clouds that penetrate into the stratocumulus deck. Drizzle first grows in cumuli, and then is transported into stratocumulus by turbulence, where it develops into heavier drizzle. The heavier drizzle breaks up the stratocumulus and removes aerosol from the boundary layer, which results in a positive feedback, and rapid conversion to drizzle in the subsequent cumulus. The drizzle creates surface divergence and produces precipitation-generated clustering of clouds. This is different from standard SCT theory, which predicts gradual erosion of stratocumulus cloud through entrainment drying by overshooting cumulus clouds. Additional simulations with a fixed cloud droplet number concentration that do produce drizzle do not show this rapid SCT induced by drizzle in cumulus. The lack of the feedback between aerosol, cloud, and precipitation effectively suppresses the enhanced drizzle formation in progressive cycles of cumulus clouds.

The ideas presented herein are, for the most part, congruent with those of PL91 who hypothesized that drizzle promotes stabilization across cloud base, which tends to dry out the cloud layer, and that drizzle also promotes a conditionally unstable subcloud layer with respect to the surface layer. These result in an unstable layer capped by a stable layer, a condition favoring moisture buildup near the surface. This state allows cumulus clouds to emerge from the unstable layer, and to penetrate into the stable cloud layer, eventually promoting the breakup of the upper stratocumulus layer. Our findings differ from PL91 on two

counts: production of drizzle occurs in the penetrative cumulus, and strong precipitation breaks up the stratocumulus.

We propose a revised SCT pathway that incorporates the ideas described above. Initially the PBL evolves following the standard SCT theory; Decoupling is formed due to a warmer SST, which promotes cumulus under stratocumulus. As long as cloud droplet size remains small (i.e., large cloud droplet number concentration), the transition continues gradually by stratocumulus dissipation through dry air entrainment by overshooting cumulus. However when the aerosol/drop concentrations become significantly eroded by progressive collision-coalescence scavenging, drizzle formation in penetrative cumulus represents a turning point at which the SCT can be rapidly accelerated by drizzle. Drizzle drops are transported into the stratocumulus where subsequent growth can form stronger drizzle. Recirculation zones in stratocumulus cloud adjacent to penetrating cumuli may also play a role in drizzle drop growth. The stronger drizzle washes out the stratocumulus and a precipitating shallow cumulus state emerges.

Simulations with varying domain sizes and advection schemes have shown that larger domains, by increasing the probability of high liquid water paths, are more conducive to precipitation formation (Figures 1 and 10). What constitutes a large enough domain size might depend on the aerosol concentration (cf., Figures 1a and 1b). The SCT is typically studied in small domains to reduce computation costs but this work shows that even the 24 km $\times$ 24 km domain used here may be too small to capture the influence of precipitation-induced mesoscale organization and its feedbacks (Figure 8). This emphasizes the need for SCT studies to balance detail in microphysical representation with domain size and dynamical core choices.

The cumulus state at the end of the simulations presented here has not reached a full trade cumulus state; for instance, it does not exhibit the well-mixed subcloud layer, positive buoyancy flux in the cloud layer, and negative buoyancy flux at cloud base. Investigations will be performed to address how these typical trade wind cumulus features form after the rapid SCT; this would inform the revised SCT scenario proposed above. Also, investigation will be conducted to identify whether rapid, drizzle-induced SCT really takes place in observed cloud systems. If so, the relative frequency of the classic SCT and the rapid SCT caused by cumulus drizzle is worth studying. New generation geostationary satellites will play an important role.

Acknowledgments
The authors thank P. Blossey for kindly providing us case configuration files and C. Bretherton for insightful discussion. Images presented in Figures 2a and 2b are produced using VAPOR (www.vapor.ucar.edu), a product of the Computational Information Systems Laboratory at the National Center for Atmospheric Research. This work is supported by NOAA's Climate Goal. Requests for the System for Atmospheric Modeling (SAM) should be directed to M. Khairoutdinov. Data of this study are available at https://esrl.noaa.gov/csd/groups/csd2/clouds.

References

Ackerman, A. S., vanZanten, M. C., Stevens, B., Savic-Jovcic, V., Bretherton, C. S., Chlond, A., . . . Zulauf, M. (2009). Large-eddy simulations of a drizzling, stratocumulus-topped marine boundary layer. *Monthly Weather Review*, *137*(3), 1083–1110. https://doi.org/10.1175/2008MWR2582.1

Albrecht, B. A., Bretherton, C. S., Johnson, D., Scubert, W. H., & Frisch, A. S. (1995). The Atlantic Stratocumulus Transition Experiment—ASTEX. *Bulletin of the American Meteorological Society*, *76*(6), 889–904. https://doi.org/10.1175/1520-0477(1995)076<0889:TASTE>2.0.CO;2

Bretherton, C. S. (1992). A conceptual model of the stratocumulus- trade-cumulus transition in the subtropical oceans. In *Proceedings of the 11th International Conference on Clouds and Precipitation* (Vol. 1, pp. 374–377). Montreal, PQ, Canada: International Commission on Clouds and Precipitation.

Bretherton, C. S., & Blossey, P. N. (2014). Low cloud reduction in a greenhouse-warmed climate: Results from Lagrangian LES of a subtropical marine cloudiness transition. *Journal of Advances in Modeling Earth Systems*, *6*, 91–114. https://doi.org/10.1002/2013MS000250

Bretherton, C. S., Blossey, P. N., & Uchida, J. (2007). Cloud droplet sedimentation, entrainment efficiency, and subtropical stratocumulus albedo. *Geophysical Research Letters*, *34*, L03813. https://doi.org/10.1029/2006GL027648

Bretherton, C. S., Krueger, S. K., Wyant, M. C., Bechtold, P., Van Meijgaard, E., Stevens, B., & Teixeira, J. (1999). A GCSS boundary-layer cloud model intercomparison study of the first ASTEX Lagrangian experiment. *Boundary-Layer Meteorology*, *93*(3), 341–380. https://doi.org/10.1023/A:1002005429969

Bretherton, C. S., & Pincus, R. (1995). Cloudiness and marine boundary layer dynamics in the ASTEX Lagrangian experiments. Part I: Synoptic setting and vertical structure. *Journal of the Atmospheric Sciences*, *52*(16), 2707–2723. https://doi.org/10.1175/1520-0469(1995)052<2707:CAMBLD>2.0.CO;2

Bretherton, C. S., & Wyant, M. C. (1997). Moisture transport, lower-tropospheric stability, and decoupling of cloud-topped boundary layers. *Journal of the Atmospheric Sciences*, *54*, 148–167. https://doi.org/10.1175/1520-0469(1997)054<0148:MTLTSA>2.0.CO;2

Chung, D., Matheou, G., & Teixeira, J. (2012). Steady-state large-eddy simulations to study the stratocumulus to shallow cumulus cloud transition. *Journal of the Atmospheric Sciences*, *69*(11), 3264–3276. https://doi.org/10.1175/JAS-D-11-0256.1

Clarke, A. D., Owens, S. R., & Zhou, J. (2006). An ultrafine sea-salt flux from breaking waves: Implications for cloud condensation nuclei in the remote marine atmosphere. *Journal of Geophysical Research*, *111*, D06202. https://doi.org/10.1029/2005JD006565

Comstock, K. K., Wood, R., Yuter, S. E., & Bretherton, C. S. (2004). Reflectivity and rain rate in and below drizzling stratocumulus. *Quarterly Journal of the Royal Meteorological Society*, *130*(603), 2891–2918. https://doi.org/10.1256/qj.03.187

Deardorff, J. W. (1980). Stratocumulus-capped mixed layers derived from a three-dimensional model. *Boundary-Layer Meteorology*, *18*, 495–527. https://doi.org/10.1007/BF00119502

de Lozar, A., & Mellado, J. P. (2016). Reduction of the entrainment velocity by cloud droplet sedimentation in stratocumulus. *Journal of the Atmospheric Sciences*, *74*(3), 751–765. https://doi.org/10.1175/JAS-D-16-0196.1

de Roode, S. R., & Duynkerke, P. G. (1997). Observed Lagrangian transition of stratocumulus into cumulus during ASTEX: Mean state and turbulence structure. *Journal of the Atmospheric Sciences*, *54*(17), 2157–2173. https://doi.org/10.1175/1520-0469(1997)054<2157:OLTOSI>2.0.CO;2

de Roode, S. R., Sandu, I., van der Dussen, J. J., Ackerman, A. S., Blossey, P., Jarecka, D., . . . Stevens, B. (2016). Large-eddy simulations of EUCLIPSEGASS Lagrangian stratocumulus-to-cumulus transitions: Mean state, turbulence, and decoupling. *Journal of the Atmospheric Sciences*, *73*(6), 2485–2508. https://doi.org/10.1175/JAS-D-15-0215.1

Durran, D. R. (1991). The third-order Adams-Bashforth method: An attractive alternative to leapfrog time differencing. *Monthly Weather Review*, *119*(3), 702–720. https://doi.org/10.1175/1520-0493(1991)119<0702:TTOABM>2.0.CO;2

Feingold, G., Koren, I., Wang, H., Xue, H., & Brewer, W. A. (2010). Precipitation-generated oscillations in open cellular cloud fields. *Nature*, *466*(7308), 849–852. https://doi.org/10.1038/nature09314

Feingold, G., Koren, I., Yamaguchi, T., & Kazil, J. (2015). On the reversibility of transitions between closed and open cellular convection. *Atmospheric Chemistry and Physics*, *15*(13), 7351–7367. https://doi.org/10.5194/acp-15-7351-2015

Feingold, G., McComiskey, A., Rosenfeld, D., & Sorooshian, A. (2013). On the relationship between cloud contact time and precipitation susceptibility to aerosol. *Journal of Geophysical Research: Atmospheres*, *118*, 10544–10554. https://doi.org/10.1002/jgrd.50819

Feingold, G., & Siebert, H. (2009). Cloud-aerosol interactions from the micro to the cloud scale. In J. Heintzenberg & R. J. Charlson (Eds.), *Clouds in the perturbed climate system: Their relationship to energy balance, atmospheric dynamics, and precipitation* (pp. 319–338). Cambridge, MA: MIT Press.

Feingold, G., Walko, R. L., Stevens, B., & Cotton, W. R. (1998). Simulations of marine stratocumulus using a new microphysical parameterization scheme. *Atmospheric Research*, *47–48*, 505–528. https://doi.org/10.1016/S0169-8095(98)00058-1

Jiang, H., Feingold, G., & Cotton, W. R. (2002). Simulations of aerosol-cloud-dynamical feedbacks resulting from entrainment of aerosol into the marine boundary layer during the Atlantic stratocumulus transition experiment. *Journal of Geophysical Research*, *107*(D24), 4813. https://doi.org/10.1029/2001JD001502

Jones, C. R., Bretherton, C. S., & Leon, D. (2011). Coupled vs. decoupled boundary layers in vocals-rex. *Atmospheric Chemistry and Physics*, *11*(14), 7143–7153. https://doi.org/10.5194/acp-11-7143-2011

Kazil, J., Wang, H., Feingold, G., Clarke, A. D., Snider, J. R., & Bandy, A. R. (2011). Modeling chemical and aerosol processes in the transition from closed to open cells during VOCALS-REx. *Atmospheric Chemistry and Physics*, *11*(15), 7491–7514. https://doi.org/10.5194/acp-11-7491-2011

Kazil, J., Yamaguchi, T., & Feingold, G. (2017). Mesoscale organization, entrainment, and the properties of a closed-cell stratocumulus cloud. *Journal of Advances in Modeling Earth Systems*, *9*. https://doi.org/10.1002/2017MS001072, in press.

Khairoutdinov, M., & Kogan, Y. (2000). A new cloud physics parameterization in a large-eddy simulation model of marine stratocumulus. *Monthly Weather Review*, *128*(1), 229–243. https://doi.org/10.1175/1520-0493(2000)128<0229:ANCPPI>2.0.CO;2

Khairoutdinov, M. F., & Randall, D. A. (2003). Cloud resolving modeling of the ARM summer 1997 IOP: Model formulation, results, uncertainties, and sensitivities. *Journal of the Atmospheric Sciences*, *60*(4), 607–625. https://doi.org/10.1175/1520-0469(2003)060<0607:CRMOTA>2.0.CO;2

Krueger, S. K., McLean, G. T., & Fu, Q. (1995). Numerical simulation of the stratus-to-cumulus transition in the subtropical marine boundary layer. Part I: Boundary-layer structure. *Journal of the Atmospheric Sciences*, *52*(16), 2839–2850. https://doi.org/10.1175/1520-0469(1995)052<2839:NSOTST>2.0.CO;2

McGibbon, J., & Bretherton, C. S. (2017). Skill of ship-following large-eddy simulations in reproducing MAGIC observations across the northeast Pacific stratocumulus to cumulus transition region. *Journal of Advances in Modeling Earth Systems*, *9*, 810–831. https://doi.org/10.1002/2017MS000924

Mlawer, E. J., Taubman, S. J., Brown, P. D., Iacono, M. J., & Clough, S. A. (1997). Radiative transfer for inhomogeneous atmospheres: RRTM, a validated correlated-k model for the longwave. *Journal of Geophysical Research*, *102*(D14), 16663–16682. https://doi.org/10.1029/97JD00237

Morrison, H. (2012). On the numerical treatment of hydrometeor sedimentation in bulk and hybrid bulk-bin microphysics schemes. *Monthly Weather Review*, *140*(5), 1572–1588. https://doi.org/10.1175/MWR-D-11-00140.1

Paluch, I. R., & Lenschow, D. H. (1991). Stratiform cloud formation in the marine boundary layer. *Journal of the Atmospheric Sciences*, *48*(19), 2141–2158. https://doi.org/10.1175/1520-0469(1991)048<2141:SCFITM>2.0.CO;2

Pawlowska, H., & Brenguier, J.-L. (2003). An observational study of drizzle formation in stratocumulus clouds for general circulation model (GCM) parameterizations. *Journal of Geophysical Research*, *108*(D15), 8630. https://doi.org/10.1029/2002JD002679

Pincus, R., Baker, M. B., & Bretherton, C. S. (1997). What controls stratocumulus radiative properties? Lagrangian observations of cloud evolution. *Journal of the Atmospheric Sciences*, *54*(17), 2215–2236. https://doi.org/10.1175/1520-0469(1997)054<2215:WCSRPL>2.0.CO;2

Rauber, R. M., Beard, K. V., & Andrews, B. M. (1991). A mechanism for giant raindrop formation in warm, shallow convective clouds. *Journal of the Atmospheric Sciences*, *48*(15), 1791–1797. https://doi.org/10.1175/1520-0469(1991)048<1791:AMFGRF>2.0.CO;2

Sandu, I., & Stevens, B. (2011). On the factors modulating the stratocumulus to cumulus transitions. *Journal of the Atmospheric Sciences*, *68*(9), 1865–1881. https://doi.org/10.1175/2011JAS3614.1

Sandu, I., Stevens, B., & Pincus, R. (2010). On the transitions in marine boundary layer cloudiness. *Atmospheric Chemistry and Physics*, *10*(5), 2377–2391. https://doi.org/10.5194/acp-10-2377-2010

Smolarkiewicz, P. K., & Grabowski, W. W. (1990). The multidimensional positive definite advection transport algorithm: Nonoscillatory option. *Journal of Computational Physics*, *86*(2), 355–375. https://doi.org/10.1016/0021-9991(90)90105-A

Stevens, B. (2000). Cloud transitions and decoupling in shear-free stratocumulus-topped boundary layers. *Geophysical Research Letters*, *27*(16), 2557–2560. https://doi.org/10.1029/1999GL011257

van der Dussen, J. J., de Roode, S. R., Ackerman, A. S., Blossey, P. N., Bretherton, C. S., Kurowski, M. J., . . . Siebesma, A. P. (2013). The GASS/EUCLIPSE model intercomparison of the stratocumulus transition as observed during ASTEX: LES results. *Journal of Advances in Modeling Earth Systems*, *5*, 483–499. https://doi.org/10.1002/jame.20033

vanZanten, M. C., Stevens, B., Nuijens, L., Siebesma, A. P., Ackerman, A. S., Burnet, F., . . . Wyszogrodzki, A. (2011). Controls on precipitation and cloudiness in simulations of trade-wind cumulus as observed during RICO. *Journal of Advances in Modeling Earth Systems*, *3*, M06001. https://doi.org/10.1029/2011MS000056

vanZanten, M. C., Stevens, B., Vali, G., & Lenschow, D. H. (2005). Observations of drizzle in nocturnal marine stratocumulus. *Journal of the Atmospheric Sciences*, *62*(1), 88–106. https://doi.org/10.1175/JAS-3355.1

Wang, H., & Feingold, G. (2009). Modeling mesoscale cellular structures and drizzle in marine stratocumulus. Part I: Impact of drizzle on the formation and evolution of open cells. *Journal of the Atmospheric Sciences*, *66*(11), 3237–3256. https://doi.org/10.1175/2009JAS3022.1

Wang, H., Feingold, G., Wood, R., & Kazil, J. (2010). Modelling microphysical and meteorological controls on precipitation and cloud cellular structures in southeast pacific stratocumulus. *Atmospheric Chemistry and Physics*, *10*(13), 6347–6362. https://doi.org/10.5194/acp-10-6347-2010

Wang, S., Albrecht, B. A., & Minnis, P. (1993). A regional simulation of marine boundary-layer clouds. *Journal of the Atmospheric Sciences*, *50*(24), 4022–4043. https://doi.org/10.1175/1520-0469(1993)050<4022:ARSOMB>2.0.CO;2

Wyant, M. C., Bretherton, C. S., Rand, H. A., & Stevens, D. E. (1997). Numerical simulations and a conceptual model of the stratocumulus to trade cumulus transition. *Journal of the Atmospheric Sciences*, *54*(1), 168–192. https://doi.org/10.1175/1520-0469(1997)054<0168:NSAACM>2.0.CO;2

Yamaguchi, T., Brewer, W. A., & Feingold, G. (2013). Evaluation of modeled stratocumulus-capped boundary layer turbulence with ship-borne data. *Journal of the Atmospheric Sciences*, *70*(12), 3895–3919. https://doi.org/10.1175/JAS-D-13-050.1

Yamaguchi, T., & Feingold, G. (2015). On the relationship between open cellular convective cloud patterns and the spatial distribution of precipitation. *Atmospheric Chemistry and Physics*, *15*(3), 1237–1251. https://doi.org/10.5194/acp-15-1237-2015

Yamaguchi, T., Feingold, G., Kazil, J., & McComiskey, A. (2015). Stratocumulus to cumulus transition in the presence of elevated smoke layers. *Geophysical Research Letters*, *42*, 10478–10485. https://doi.org/10.1002/2015GL066544

Yamaguchi, T., Randall, D. A., & Khairoutdinov, M. F. (2011). Cloud modeling tests of the ultimate-macho scalar advection scheme. *Monthly Weather Review*, *139*(10), 3248–3264. https://doi.org/10.1175/MWR-D-10-05044.1